

FIRST ELECTROMAGNETIC PULSE ASSOCIATED WITH A GRAVITATIONAL-WAVE EVENT: PROFILE, DURATION, AND DELAY

DA-BIN LIN¹, TONG LIU², JIE LIN¹, XIANG-GAO WANG¹, WEI-MIN GU², AND EN-WEI LIANG¹

¹Laboratory for Relativistic Astrophysics, Department of Physics, Guangxi University, Nanning 530004, China; lindabin@gxu.edu.cn

²Department of Astronomy, Xiamen University, Xiamen, Fujian 361005, China

ABSTRACT

We study the first electromagnetic pulse after the gravitational wave chirp signal, focusing on the profile and duration. It is found that the light curve, especially the steep decay (SD) phase, can be very different by adopting different viewing angle θ_{view} on the jet shell. For an on-axis jet with a power-law radiation spectrum, the observed flux in the SD is proportional to $t_{\text{obs}}^{-2-\beta}$ with β being the spectral index and t_{obs} being the observer time. Here, $t_{\text{obs}} = 0$ is set at the observed time of the jet ejected from the central engine. The SD may become steep by increasing θ_{view} . We also study the bolometric luminosity L from a jet shell with a non-power-law radiation spectrum. For an on-axis jet, $L \propto t_{\text{obs}}^{-3}$ is found in the SD. However, the SD is steeper than $L \propto t_{\text{obs}}^{-3}$ for the radiation from an off-axis jet. The higher value of θ_{view} is, the steeper of SD would be. Then, we suggest that the SD phase can be used to discriminate an off-axis jet from an on-axis jet. The reason for above behaviors is discussed. In addition, we find that the duration of first electromagnetic pulse is close to its peak time, especially for $\theta_{\text{view}} \sim 20^\circ$. This result is consistent with that found in GW 170817/GRB 170817A. Thus, the jet corresponding to the prompt emission of GRB 170817A should be immediately ejected after the merger. Our results also reveal that the duration of the first electromagnetic pulse can provide the information of the time to search gravitational waves.

Keywords: gamma-ray burst: general — stars: neutron — gravitational waves — gamma-ray burst: individual (GRB 170817A)

1. INTRODUCTION

For the first time, gravitational wave (GW) and electromagnetic (EM) wave from a single source have been observed. On August 17, 2017 at 12:41:04 UTC, the Advanced Laser Interferometer Gravitational-wave Observatory and the Advanced Virgo gravitational-wave detectors have made their first observation on a binary neutron star (NS) merger (Abbott et al. 2017a,b,c,d). The associated gravitational radiation event is known as GW 170817. About 2 seconds after GW 170817, the Fermi Gamma-ray Burst Monitor (GBM) has autonomously detected a short gamma-ray burst (GRB), GRB 170817A, from a location coincident with GW 170817 (Goldstein 2017). GRB 170817A was also detected by the International Gamma-Ray Astrophysics Laboratory (Savchenko et al. 2016; He et al. 2017). These observations were followed by a detection of an optical counterpart, SSS17a (now with the IAU identification of AT2017gfo, Coulter 2017), associated with the accompanying Macronova/kilonova powered by the radioactive decay of heavy elements formed in the NS-NS merger (Li & Paczyński 1998; Metzger & Berger 2012; Berger et al. 2013; Fernández & Metzger 2016; Ma et al. 2017; Song & Liu 2017; Liu et al. 2017). In addition, the accompanying Macronova/kilonova was independently confirmed by several teams (e.g., Abbott et al. 2017a; Arcavi et al. 2017; Hu et al. 2017; Lipunov et al. 2017; Soares-Santos et al. 2017; Tanvir et al. 2017; Valenti et al. 2017; Smartt et al. 2017; Troja et al. 2017; Hallinan et al. 2017). The joint GW-EM detection has provided the first compelling observational evidence on the relation of short GRBs and NS-NS mergers and has led to the new era of gravitational-wave multi-messenger astrophysics.

The NS-NS merger is due to the loss of orbital energy and angular momentum via gravitational radiation. The merger of two NSs can have four possible outcomes (Abbott et al. 2017e): (i) The prompt formation of a black hole (BH); (ii) the formation of a hypermassive NS collapsing to a BH with $\lesssim 1$ s; (iii) the formation of a supramassive NS collapsing to a BH with $\sim 10 - 10^4$ s, or (iv) the formation of a stable NS. Accretion onto the formed BH can launch a relativistic jet and thus powers a GRB. GRB 170817A was indeed found after GW 170817. GRB 170817A triggered Fermi GBM with a duration of $T_{90} = 2$ s (Abbott et al. 2017a; Fraija et al. 2017b; He et al. 2017). The prompt γ -ray

of GRB 170817A is faint and peaks at ~ 2.1 s after the GM chirp signal (Abbott et al. 2017a; Fraija et al. 2017b; He et al. 2017). In addition, a fast decay appears in the light curve of GRB 170817A after the peak time. The physical origin of the prompt emission in GRB 170817A is still under debate. The prompt emission in GRB 170817A may be formed in the photosphere of the jet (Meng et al. 2018), the internal shocks (Murguía-Berthier et al. 2017), the internal-collision-induced magnetic reconnection and turbulence (Meng et al. 2018; Zhang & Yan 2011), or the external-reverse shock (RS, Fraija et al. 2017b). Except the radiation spectrum, these models should explain why there is not variability associated with this burst. The emission from the reverse shock is exhibited as a single peak and thus can easily explain the single peaked behavior of GRB 170817A (Fraija et al. 2017b). The internal shock model, the pulse width is Doppler contracted, while the pulse separation is not. Then a sizable increase in the viewing angle would cause significant overlap between pulses and, as a result, the variability would be washed out (Salafia et al. 2016). The onset and peak time of GRB 170817A also drew a significant attention. For example, the delay of EM signal relative to the GW chirp signal has been used to constrain the remnants of the NS-NS merger (Granot et al. 2017), the weak equivalence principle (Wei et al. 2017; Shoemaker & Murase 2017; Wang et al. 2017), and the velocity of GW (Wang et al. 2017). In this paper, however, we would like to point out that the peak time (t_p) of the first EM pulse is close to the duration (T_{90}) of this pulse if the jet is immediately launched after the GW chirp signal. In GW 170817/GRB 170817A, $t_p \sim T_{90}$ is found. Then, we would like to believe that the jet associated with GRB 170817A is immediately launched after the NS-NS merger. This result should be considered in utilizing the EM wave-GW delay in constraining the associated physical processes. We also study the light curves of the first EM pulse. It is found that the steep decay (SD) can be used to discriminate an off-axis jet emission from an on-axis jet emission.

The paper is organized as follows. Since we study the radiation of the jet shell via a Monte Carlo method, the procedure for simulating jet emission is presented in Section 2. The light curves and other results are presented in Section 3. The conclusions and discussions are presented in Section 4.

2. PROCEDURE FOR SIMULATING JET EMISSION

We focus on the radiation of a spherical thin jet shell radiating from r_0 to r_e , where r_0 and r_e are estimated with respect to the jet base ($r = 0$). This process can appear in the internal shocks (Rees & Meszaros 1994), the internal-collision-induced magnetic reconnection and turbulence (Zhang & Yan 2011; Deng et al. 2015), or the RS shock (e.g., Shao & Dai 2005; Kobayashi et al. 2007; Fraija 2015; Fraija et al. 2016a,b, 2017a,b), especially for a radiating jet shell with a fast decaying behavior after the peak. The jet shell (yellow region) is schematically shown in Figure 1, where the spherical coordinate with $r = 0$ locating at the central engine of GRB and $\theta = 0$ being along the line of sight is adopted, θ_{jet} is the jet opening angle, and θ_{view} is the viewing angle of the jet shell. The jet shell is assumed uniform with sharp edges.

The radiation of our jet shell is computed via a Monte Carlo method (e.g., Lin et al. 2017a,b). In brief, a number of emitters randomly distributed in the jet shell is used to simulate the radiation of the jet shell. The radiation of an emitter in the jet shell comoving frame is assumed as (e.g., Uhm & Zhang 2015)

$$P'(E') = P'_0 H'(E'/E'_0), \quad (1)$$

where P'_0 describes the spectral power and E'_0 is the characteristic photon energy of the radiation spectrum. For the function form of H' , we study the following three cases:

$$\begin{aligned} \text{Case (I) :} & \quad H'(x) = x^{\hat{\beta}+1}, \\ \text{Case (II) :} & \quad H'(x) = \begin{cases} x^{\hat{\alpha}+1} \exp(-x), & x \leq (\hat{\alpha} - \hat{\beta}), \\ (\hat{\alpha} - \hat{\beta})^{\hat{\alpha}-\hat{\beta}} \exp(\hat{\beta} - \hat{\alpha}) x^{\hat{\beta}+1}, & x \geq (\hat{\alpha} - \hat{\beta}), \end{cases} \\ \text{Case (III) :} & \quad H'(x) = x^{\hat{\alpha}} \exp(-x), \end{aligned} \quad (2)$$

where $\hat{\alpha}$ and $\hat{\beta}$ are spectral indexes. A photon in the comoving frame with energy E' is boosted to $E = DE'/(1+z)$ in the observer's frame. Here, z is the redshift of the GRB and D is the Doppler factor described as

$$D = [\Gamma(1 - v_{\text{jet}} \cos \theta/c)]^{-1} \quad (3)$$

with c , θ , $v_{\text{jet}} = dr/dt$, and $\Gamma = 1/\sqrt{1 - (v_{\text{jet}}/c)^2}$ being the light velocity, the latitude of the radiating emitter, the jet shell velocity, and the jet shell Lorentz factor, respectively. During the shell's expansion for δt (~ 0) from r to $r + v_{\text{jet}}\delta t$, the observed spectral energy δU from an emitter into a solid angle $\delta\Omega$ is given as (Uhm & Zhang 2015)

$$\delta U_E(t_{\text{obs}}) = (D^2 \delta\Omega) \left(\frac{\delta t}{\Gamma} \right) \frac{1}{4\pi} P'_0 H' \left(\frac{E(1+z)}{DE'_0} \right), \quad (4)$$

where the radiation is assumed isotropically in the jet shell comoving frame (c.f. [Geng et al. 2017](#)). The observed time of δU is estimated with

$$t_{\text{obs}} = \left\{ \int_{r_0}^r [c - v_{\text{jet}}] \frac{dl}{cv_{\text{jet}}(l)} + \frac{r(1 - \cos \theta)}{c} \right\} (1 + z) + t_{\text{obs},r_0}, \quad (5)$$

where θ is the latitude of the radiating emitter. In our work, $t_{\text{obs}} = 0$ is set at the observed time of the jet shell ejected from $r = 0$, and thus t_{obs,r_0} is the observed time of the emitter locating at r_0 and $\theta = 0$.

The procedures of our simulations to obtain the observed flux is shown as follows. Firstly, an expanding jet is modelled with a series of jet shells at radius r_0 , $r_1 = r_0 + v_{\text{jet}}\delta t$, $r_2 = r_1 + v_{\text{jet}}\delta t$, \dots , $r_n = r_{n-1} + v_{\text{jet}}\delta t$, \dots appearing at the time $t = 0s$, δt , $2\delta t$, \dots , $n\delta t$, \dots , respectively. During the shell's expansion for δt , the shell moves from r_{n-1} to r_n with the same radiation behavior for emitters. Secondly, we produce N emitters centred at $(r_n, \theta_{\text{sh}}, \varphi_{\text{sh}})$ in spherical coordinates with $\theta_{\text{sh}} = 0$ being along the axis of the jet shell, where the value of $\cos \theta_{\text{sh}}$ and φ_{sh} are randomly picked up from linear space of $[\cos \theta_{\text{jet}}, 1]$ and $[0, 2\pi]$, respectively. Then, the value of $\cos \theta$ can be estimated with

$$\cos \theta = \sin \theta_{\text{sh}} \cos \varphi_{\text{sh}} \sin \theta_{\text{view}} + \cos \theta_{\text{sh}} \cos \theta_{\text{view}}. \quad (6)$$

The observed spectral energy from an emitter during the shell's expansion from r_{n-1} to r_n is calculated with Equation (4). By discretizing the observer time t_{obs} into a series of short time intervals, i.e., $[0, t_{\text{obs},1}]$, $[t_{\text{obs},1}, t_{\text{obs},2}]$, \dots , $[t_{\text{obs},k-1}, t_{\text{obs},k}]$, \dots , we can find the total observed spectral energy

$$U_E|_{[t_{\text{obs},k-1}, t_{\text{obs},k}]} = \sum_{t_{\text{obs},k-1} \leq t_{\text{obs}} < t_{\text{obs},k}} \delta U_E(t_{\text{obs}}) \quad (7)$$

in the time interval $[t_{\text{obs},k-1}, t_{\text{obs},k}]$ based on Equations (4) and (5). Then, the observed flux F_E at the observer time $(t_{\text{obs},k-1} + t_{\text{obs},k})/2$ can be estimated as

$$F_E = \frac{U_E|_{[t_{\text{obs},k-1}, t_{\text{obs},k}]}}{D_L^2(t_{\text{obs},k} - t_{\text{obs},k-1})\delta\Omega}, \quad (8)$$

where D_L is the luminosity distance of the jet shell with respect to the observer. The bolometric luminosity L is written as

$$L = 4\pi D_L^2 \int_0^\infty F_E dE. \quad (9)$$

In our simulations, the jet shell is assumed to radiate from $r_0 = 10^{12}$ cm to $r_e = 2r_0$ with a Lorentz factor $\Gamma = 100$ and $E'_0 = 150\text{keV}(1+z)/D_0$, where $D_0 = 2\Gamma$ and $D_0 = 1/\Gamma[1 - \beta \cos(\theta_{\text{view}} - \theta_{\text{jet}})]$ are adopted for $\theta_{\text{view}} \leq \theta_{\text{jet}}$ and $\theta_{\text{view}} > \theta_{\text{jet}}$, respectively. Thus, $t_{\text{obs},r_0} = r_0/2\Gamma^2 c$ can be estimated. The value of P'_0 is assumed to increase with time t' in the jet comoving frame, i.e., $P'_0 = P'_{0,0}t'$ with constant $P'_{0,0}$, and $t' = 0$ is set at the situation that the jet shell arrives at r_0 . The value of $N \gg 1$, $\theta_{\text{jet}} = 5^\circ$, and $z = 1$ are adopted and remain constant in our simulations.

3. FIRST ELECTROMAGNETIC PULSE AFTER GRAVITATIONAL CHIRP SIGNAL

In Figure 2, we show the light curves of the first EM pulse after GW chirp signal by varying θ_{view} , where Case (I) with $\hat{\beta} = -1.3$ is adopted in our simulations and t_p (F_p) is the peak time (flux) of the light curve. The situations with $\theta_{\text{view}} = 0^\circ, 5^\circ, 10^\circ, 20^\circ, 40^\circ$, and 60° are represented with the black, red, orange, yellow, green, and blue lines, respectively. Similar to the results in [Yamazaki et al. \(2003\)](#), the light curves from our simulations with different θ_{view} can be very different, especially for those in the SD phase (i.e., $t_{\text{obs}} > t_p$). Then, we focus our attention on the SD. For the light curves from our simulations, the SD is shaped by the shell curvature effect, which is a combination of the time delay and the Doppler shifting of the intrinsic radiation spectrum for high latitude (θ) emission with respect to the emission from low latitude. For the radiation from an on-axis jet shell with Case (I), the light curves of the SD phase have been well studied (e.g., [Kumar & Panaitescu 2000](#); [Dermer 2004](#); [Dyks et al. 2005](#); [Uhm & Zhang 2015](#); [Lin et al. 2017a,b](#)). The well-known relation, $\alpha = \beta + 2$, has been derived in the SD phase, where the value of $-\alpha$ is the power law decay index (i.e., $F \propto t_{\text{obs}}^{-\alpha}$) and β is the spectral index. Then, we plot the light curve (cyan dashed line) of $F \propto t_{\text{obs}}^{-\beta-2}$ in the right panel of Figure 2, where $\beta = -\hat{\beta}$ is obtained for the simulations with Case (I). It can be found that the light curve in the SD phase may deviate from $F \propto t_{\text{obs}}^{-\beta-2}$ for the simulations with high θ_{view} . The higher value of θ_{view} we adopt, the more obvious the deviation would appear. Then, we suggest that the SD can be used to discriminate an off-axis jet from an on-axis jet. We also study the light curves in the situations with Case (II) or (III). In these situations, however, the relation of α and β is complex in the SD phase due to the evolution of β (see [Lin et al. 2017a,b](#)). Then, we study the light curves of the bolometric luminosity L in Figure 3, where L_p is the peak

luminosity. For a SD shaped by the curvature effect, the light curves can be described as $L \propto t_{\text{obs}}^{-3}$ for an on-axis jet shell. Then, we show the relation of $L \propto t_{\text{obs}}^{-3}$ in Figure 3 with cyan dashed lines. The meanings of other lines in Figure 3 are the same as those in Figure 2. One can find that the luminosity in the SD phase also deviates from $L \propto t_{\text{obs}}^{-3}$ for the situations with high θ_{view} . The higher value of θ_{view} we take, the more obvious the deviation would be. We also perform spectral fittings and obtain the value of E_0 (E_c) for the simulations with Case (II) or (III). The obtained E_0 (E_c) is shown in the left panels of Figure 4 and almost consistent with $E_0 \propto t_{\text{obs}}$ ($E_c \propto t_{\text{obs}}$) in the SD phase, where $E_0 \propto t_{\text{obs}}$ ($E_c \propto t_{\text{obs}}$) is shown with a cyan dashed line. The right panels of Figure 4 show the relations of $L - E_c$ (upper-right panel) and $L - E_0$ (lower-right panel) in the SD phase. One can find that the relation of $L - E_0$ ($L - E_c$) deviates from $L \propto E_0^3$ ($L \propto E_c^3$) for the simulations with high θ_{view} , where $L \propto E_0^3$ ($L \propto E_c^3$) is shown with a cyan dashed line. In Figure 4, the meanings of other lines are the same as those in Figure 2. The higher value of θ_{view} is, the steeper of $L - E_c$ ($L - E_0$) would be. Then, we conclude that the SD can be used to estimate the viewing angle θ_{view} .

The reason for above found deviations is shown as follows. According to Figures 2 and 3, one can find that the deviation of the SD from the cyan dashed line only become evident in the simulations with $\theta_{\text{view}} > \theta_{\text{jet}}$. Then, we discuss the situations with $\theta_{\text{view}} > \theta_{\text{jet}}$. For the radiation from the dotted region (see Figure 1), the evolution of L can be described as (Lin et al. 2017a)

$$L \propto \left(1 + \frac{t_{\text{obs}} - t_0}{t_c}\right)^{-3}, \quad (10)$$

where

$$t_c(r) = \left\{ \frac{r}{2\Gamma^2 c} + \frac{r}{c} [1 - \cos(\theta_{\text{view}} - \theta_{\text{jet}})] \right\} (1 + z) \quad (11)$$

is the angular spreading timescale for the radiation from the dotted region and $t_0 (= t_c)$ is the observed time of the first photon from the dotted region. The dotted region in Figure 1 is an annulus with $\theta \in [\theta_{\text{view}} - \theta_{\text{jet}}, \theta_{\text{view}} + \theta_{\text{jet}}]$ and swaddled by two longitude l_E and l_W , where l_E and l_W are tangent to the jet shell at the latitude θ_c . From Figure 1, one can find that the covered dotted region by the jet shell increases with θ for $\theta < \theta_c$ and decreases with θ for $\theta > \theta_c$. Then, the evolution of L relative to t_{obs} may be shallower than that of Equation (10) at the early phase of the SD and steeper than that of Equation (10) at the later phase of the SD. These behaviors can be found in the situations with $\theta_{\text{view}} = 10^\circ$ and 20° . Furthermore, the total duration of the SD phase can be read as

$$t_d = (1 + z) \frac{r}{c} [\cos(\theta_{\text{view}} - \theta_{\text{jet}}) - \cos(\theta_{\text{view}} + \theta_{\text{jet}})]. \quad (12)$$

A sharp cutoff would appear in the light curve at $t_{\text{obs}} \gtrsim t_d$. It should be noted that the value of t_d/t_c decreases with increasing θ_{view} based on Equations (11) and (12). This behavior can be found in Figure 5, where the black, red, and blue solid lines represent the value of t_d/t_c calculated with $\Gamma = 50, 150, 450$, respectively. In addition, the $\theta_{\text{jet}} = 5^\circ$ (10°) is adopted in the left (right) panel and the green dashed line represents $t_d = t_c$. According to this figure, $t_d < t_c$ appears at $\theta_{\text{view}} \gtrsim 30^\circ$ (55°) in the simulations with $\theta_{\text{jet}} = 5^\circ$ (10°). Then, the SD would quickly enter into the sharp cutoff phase for $\theta_{\text{view}} \gtrsim 30^\circ$ (55°) in the simulations with $\theta_{\text{jet}} = 5^\circ$ (10°). This behavior can be easily found in the light curves from the simulations with $\theta_{\text{view}} = 40^\circ$ or 60° . By varying θ_{jet} , we show the value of θ_{view} satisfying $t_d = t_c$ in Figure 6, where $\Gamma = 150$ is adopted in our calculation. One should note that the value of Γ ($\gtrsim 50$) does not affect the obtained θ_{view} , which can be found in Figure 5. Figure 6 suggests that the sharp cutoff is more likely to appear in the SD shaped by an off-axis jet shell with a low θ_{jet} . One would note that the onset of afterglow may overlap in time with the SD of the prompt emission (O'Brien et al. 2006; Fraija et al. 2017), especially for an on-axis jet. For an off-axis jet shell, the variability timescale of the prompt emission, the peak time of the afterglow onset, and the separation between the prompt emission and the afterglow onset is proportional to $\Gamma[1 - v_{\text{jet}} \cos(\theta_{\text{view}} - \theta_{\text{jet}})/c]$. As discussed above, however, the sharp cutoff may quickly appear in the situation with an off-axis jet and thus the SD and the afterglow onset can be well separated. That is to say, one can easily identify the SD of prompt emission and the afterglow onset for an off-axis jet.

0

In our simulations, the jet shell is radiating from r_0 to r_e with P'_0 increasing with t' . In this situation, the SD is dominated by the radiation from the jet shell located at r_e and the peak time of luminosity would be at $\sim t_0(r_e)$, i.e., $t_p \sim t_0(r_e) = t_c(r_e)$. This is to say, the value of the peak time for the first EM pulse is close to the decay timescale of the SD phase. Then, one would expect that the duration of the first EM pulse would be close to the value of the peak time of the first EM pulse. In Figure 7, we study the relation of T_{90} and t_p for the light curves plotted in Figures 2 and 3, where the symbols of “o”, “+”, and “x” represent the results from the simulations with Case (I),

(II), and (III), respectively. From Figure 7, the $0.4 \lesssim T_{90}/t_p \lesssim 3$ can be found. In addition, $T_{90} \sim t_p$ can be easily found for $\theta_{\text{view}} = 20^\circ$. This result is consistent with the EM wave-GW delay found in GW 170817/GRB 170817A. The delay of the first EM pulse with respect to the GW chirp signal can be decomposed into three components: (1) the time for the jet formation, which can be neglected for GW 170817/GRB 170817A (e.g., Zhang et al. 2017); (2) the time for the jet propagating from the central engine to the dissipation location; (3) the geometrical delay, $\Delta t_g = (1+z)[1 - \cos(\theta_{\text{view}} - \theta_{\text{jet}})]r/c$, which is induced by the additional path of the jet edge relative to the light of sight and only appears in the situation of $\theta_{\text{view}} > \theta_{\text{jet}}$. For a high viewing angle θ_{view} , the delay induced by (2) is less than that induced by (3). Then, the delay of the first EM pulse relative to the GW chirp signal would be dominated by $\Delta t_g \sim t_c$. This is the reason for the consistency of our obtained delay with that found in GW 170817/GRB 170817A. Then, we conclude that the lead of GW chirp signal with respect to the EM pulse is around the duration of the first EM pulse.

4. CONCLUSIONS AND DISCUSSIONS

In this work, we study the light curve of the first electromagnetic pulse after gravitational wave chirp signal. We find that the light curve, especially the steep decay phase, can be very different for different viewing angle θ_{view} . In our work, the SD is shaped by the shell curvature effect. For the radiation from an on-axis jet shell with a power-law intrinsic radiation spectrum, the light curves in the SD will follow $F_\nu \propto t_{\text{obs}}^{-2-\beta}$ with β being the spectral index. However, the light curves deviate from $F_\nu \propto t_{\text{obs}}^{-2-\beta}$ for the situation with high θ_{view} . The higher value of θ_{view} is, the more obvious the deviation would be. We also study the bolometric luminosity from an radiating jet shell with a non-power-law radiation spectrum. In this situation, the bolometric luminosity in the SD can be described as $L \propto t_{\text{obs}}^{-3}$ for an on-axis jet shell. For an off-axis jet shell, the luminosity in the SD also deviates from $L \propto t_{\text{obs}}^{-3}$. The higher value of θ_{view} we adopt, the more obvious the deviation would appear. Then, we conclude that the SD can be used to discriminate between an on-axis jet radiation and an off-axis jet radiation. We also present the explanation for the above found deviations. In addition, it is found that the duration of the first EM pulse is close to the value of its peak time, especially for the situation with $\theta_{\text{view}} \sim 20^\circ$. This result is consistent with the EM wave-GW delay found in GW 170817/GRB 170817A. Thus, the jet corresponding to the prompt emission of GRB 170817A should be immediately ejected after the NS-NS merger. Our results also reveal that the duration of the first EM pulse can provide the searching time for gravitational chirp signal in a GW event associated with a GRB.

A structured jet is usually used to fit the afterglow of GW 170817/GRB 170817A (e.g., Lazzati et al. 2017; Meng et al. 2018; Lyman et al. 2018). **To explain the EM wave-GW delay found in GW 170817/GRB 170817A, however, a significant delay between the NS-NS merger and the launch of the jet is required in this scenario (e.g., Meng et al. 2018). In this situation, the value of T_{90} would be significantly less than that of t_p based on our obtained results. This behavior is inconsistent with the observations (i.e., $T_{90} \sim t_p$).** Furthermore, it should be noted that the jet structure in the prompt emission phase and that in the later afterglow phase can be very different due to the lateral expansion of the jet (e.g., Rhoads 1997, 1999; Huang et al. 2000). Then, a structured jet may well explain the afterglow emission but is not a required ingredient in explaining the prompt emission. Our found relation between T_{90} and t_p is applicable for a radiating jet shell in the internal shocks (Rees & Meszaros 1994), the internal-collision-induced magnetic reconnection and turbulence (Zhang & Yan 2011; Deng et al. 2015), or the RS shock (e.g., Shao & Dai 2005; Kobayashi et al. 2007; Fraija 2015; Fraija et al. 2016a,b, 2017a,b), especially for those with a fast decaying behavior after the peak. The light curves formed in the external-forward shock always has a normal decay with power-law decay index ~ -1.2 (e.g., Zhang et al. 2006). In this situation, one could not define T_{90} and the value of T_{90}/t_p . Then, our model is not applicable for the external-forward shock. Several GRBs with a flash formed in the RS shock are identified, e.g., GRBs 990123 (Akerlof et al. 1999), 041219A (Blake et al. 2005; Vestrand et al. 2005), 050820A (Vestrand et al. 2006), 090102 (Steele et al. 2009), 090510 (Fraija et al. 2016b; Ackermann et al. 2010), 110731A (Fraija 2015; Ackermann et al. 2013), 130427A (Vestrand et al. 2014; Fraija et al. 2016a), 140512A (Huang et al. 2016), and 160625B (Zhang et al. 2016; Lü et al. 2017; Fraija et al. 2017a). Table 1 shows the value of T_{90} , t_p , and T_{90}/t_p for the RS flash in these bursts, where the trigger time of the burst is set as the zero time. The relation of $T_{90} \sim t_p$ can be easily found. We would like to point out that, for flashes formed in a same RS, one can have $T_{90} \sim 3t_p$ for the flash observed in the optical band if $T_{90} \sim 0.5t_p$ is obtained for the flash observed in the Fermi-LAT band. This conclusion is obtained based on the observations of GRB 130427A. In this burst, the $T_{90} \sim 4.66t_p$ ($T_{90} \sim 0.26t_p$) is found for the optical (Fermi-LAT) flash, which is explained through synchrotron (synchrotron self-Compton) emission from the RS. Then, one can have $T_{90} \sim 3t_p$ for the RSs listed in Table 1 and observed in the optical band. These results reveal that the jet in GRBs listed in Table 1 would be in the on-axis situation rather than off-axis situation.

The relation between T_{90} and t_p can be used to estimate the ejection time of the jet. In Table 1, GRBs 050820A and 160625B are not discussed since the trigger time of the burst is not the zero time of our focused RS flash. The energy injection into the external shock is discussed in these two bursts, e.g., Vestrand et al. (2006), Fraija et al. (2017a), and Lin et al. (2018). Central engines of GRBs may be intermittent and launch several episodes of ejecta separated by a long quiescent interval. In this scenario, an external shock is formed due to the propagation of the first launched ejecta into the circum-burst medium and the later launched ejecta may interact with the external shock at a later period. Then, the onset of the dominant afterglow component should be referenced to the time of the onset of the dominant γ -ray pulse, especially for GRBs with a weak precursor, e.g., GRB 160625B. Based on the observations of the optical flash (Zhang et al. 2016; Lü et al. 2017), we have $T_{90} \sim 73$ s and $t_p = 207$ s. Then, the ejected time of this ejecta is at around $t_p - T_{90}/3 \sim 183$ s, which is the beginning of the second sub-burst in GRB 160625B and consistent with that found in Fraija et al. (2017a). It is interesting to point out that the ejection time of an on-axis jet shell can be exactly estimated by fitting the SD (Lin et al. 2017a). In Lin et al. (2017a), we move the zero time t_0 to a certain time in the SD phase and derive an analytical formula to describe the bolometric luminosity evolution, i.e., Equation (10) in this paper. For a coasting jet shell, the $t_0 - t_c$ is corresponding to the observed time of the jet shell ejected from the central engine. One can use Equation (10) to fit the SD of the first EM pulse and obtain the value of t_c . If $t_0 - t_c$ lags behind the observed time of GW chirp signal, the first EM pulse may be produced in an off-axis jet shell. This is another method to judge the jet being on-axis or off-axis.

This work is supported by the National Basic Research Program of China (973 Program, grant No. 2014CB845800), the National Natural Science Foundation of China (grant Nos. 11773007, 11403005, 11533003, 11673006, 11573023, 11473022), the Guangxi Science Foundation (grant Nos. 2016GXNSFDA380027, 2016GXNSFFA380006), the Special Funding for Guangxi Distinguished Professors (Bagui Yingcai & Bagui Xuezhe), the Innovation Team and Outstanding Scholar Program in Guangxi Colleges, and the One-Hundred-Talents Program of Guangxi colleges.

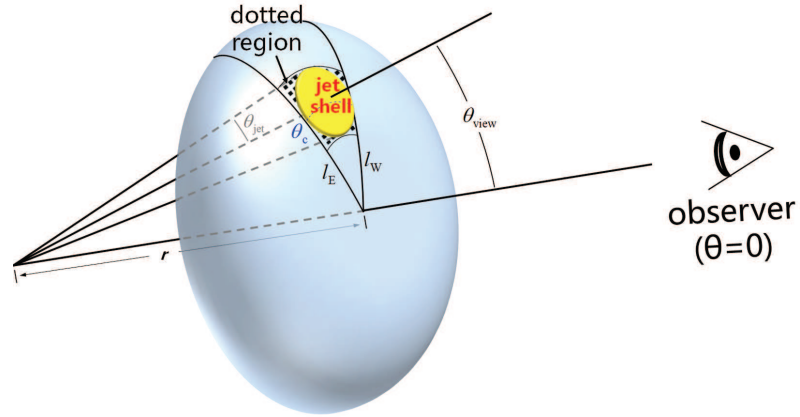


Figure 1. Illustration of our radiating jet shell (yellow region). Here, the spherical coordinate with $r = 0$ locating at the central engine of GRB and $\theta = 0$ being along the line of sight is adopted, θ_{jet} is the jet opening angle, and θ_{view} is the viewing angle of the jet shell axis. The dotted region is an annulus with $\theta \in [\theta_{\text{view}} - \theta_{\text{jet}}, \theta_{\text{view}} + \theta_{\text{jet}}]$ and swaddled by two longitudes l_E and l_W , where l_E and l_W are tangent to the jet shell at the latitude θ_c .

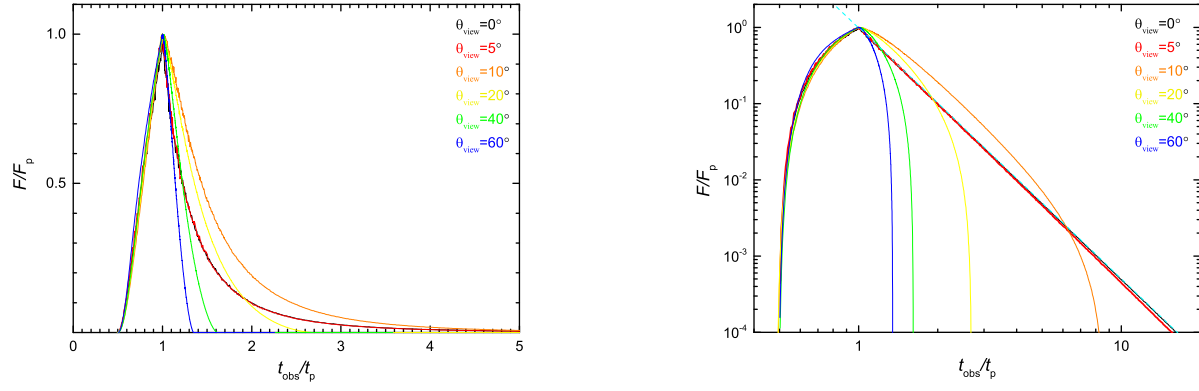


Figure 2. Light curves of the first electromagnetic pulse, where the black, red, orange, yellow, green, and blue solid lines represent the situations with $\theta_{\text{view}} = 0^\circ, 5^\circ, 10^\circ, 20^\circ, 40^\circ,$ and 60° , respectively. The cyan dashed line in the right panel plots the relation of $F \propto t_{\text{obs}}^{-2-\beta}$.

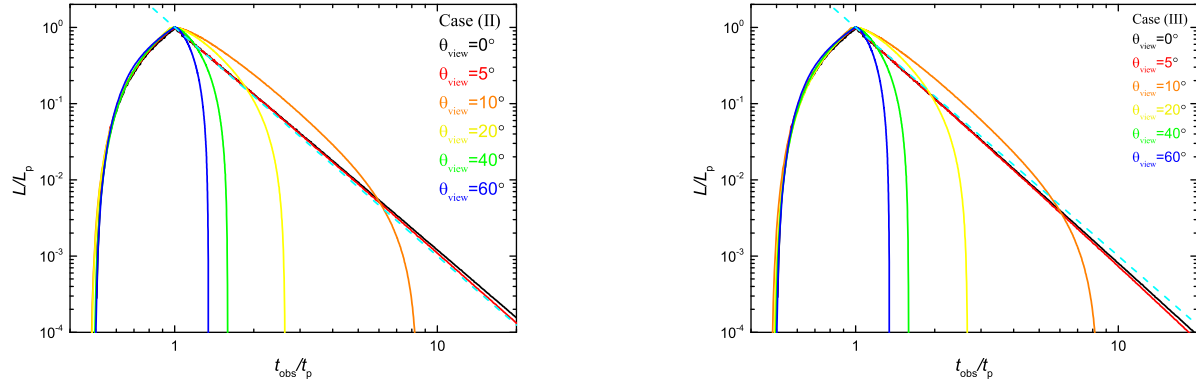


Figure 3. Luminosity of an radiating jet shell with Case (II) (left panel) and Case (III) (right panel), where the black, red, orange, yellow, green, and blue solid lines represent the situations with $\theta_{\text{view}} = 0^\circ, 5^\circ, 10^\circ, 20^\circ, 40^\circ,$ and 60° , respectively. The cyan dashed lines plot the relation of $L \propto t_{\text{obs}}^{-3}$.

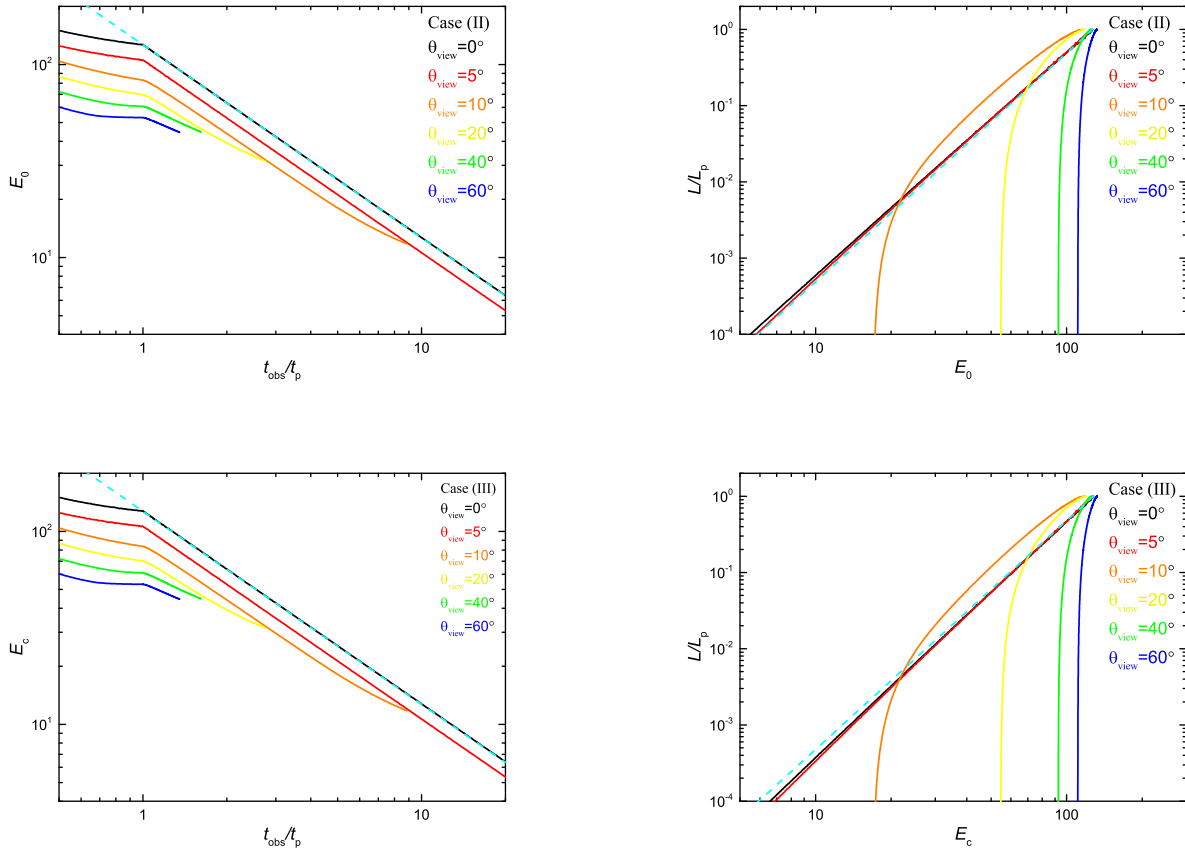


Figure 4. Evolution of E_0 (E_c) and relations of $L - E_0$ ($L - E_c$). A 1.2 shift between two adjacent $E_0 - t_{\text{obs}}$ ($E_c - t_{\text{obs}}$) is applied in the plot for clarity.

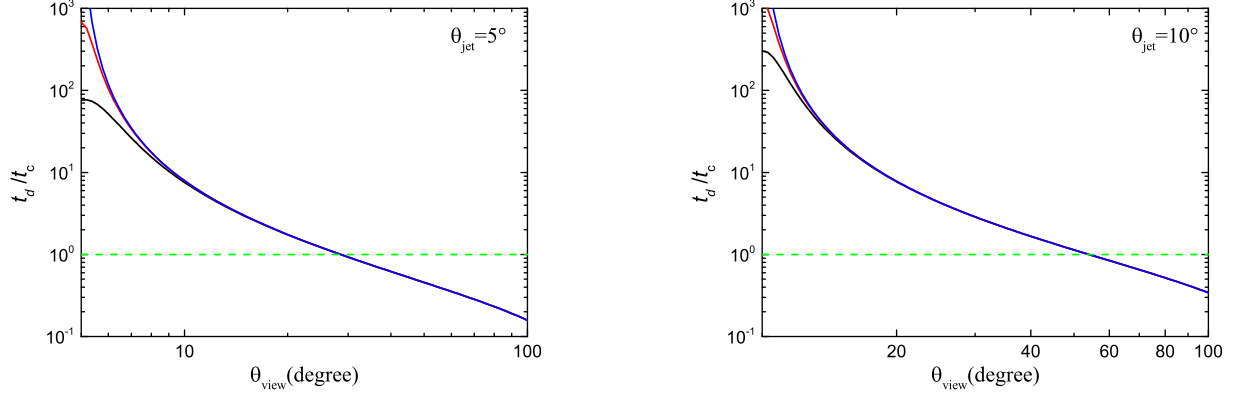


Figure 5. Value of t_d/t_c for different θ_{view} , where the black, red, and blue solid lines represent the value of t_d/t_c calculated with $\Gamma = 50, 150, 450$, respectively. In addition, $\theta_{\text{jet}} = 5^\circ$ (10°) is adopted in the left (right) panel and the green dashed lines represent $t_d = t_c$.

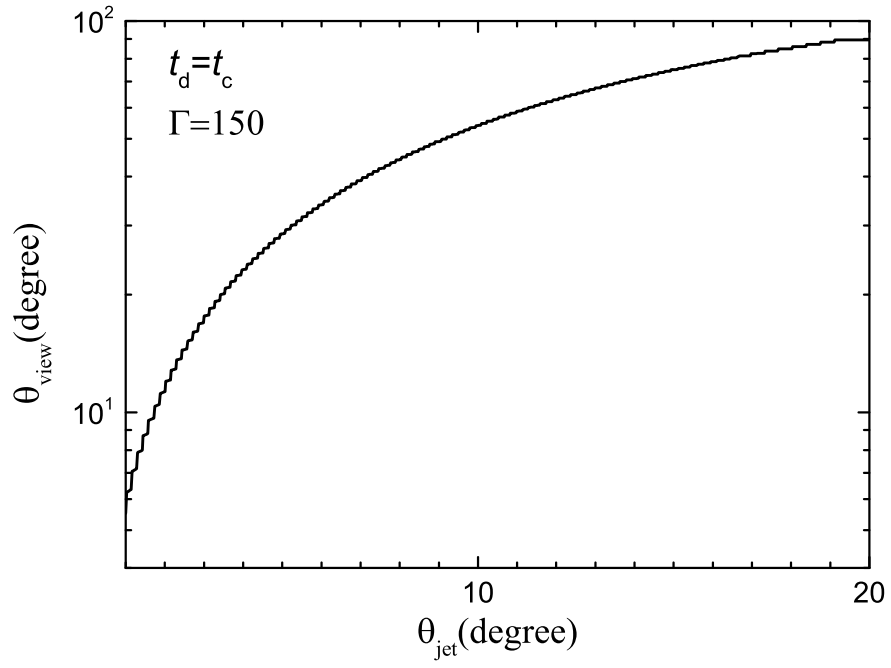


Figure 6. Value of θ_{view} satisfying $t_d = t_c$ for different θ_{jet} , where $\Gamma = 150$ is adopted.

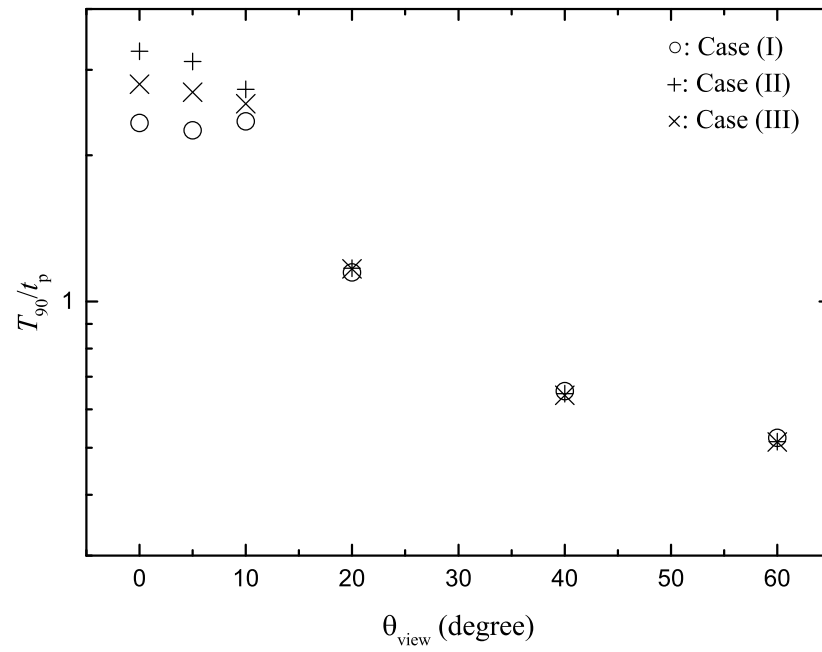


Figure 7. Relation of T_{90} and t_p for different viewing angle, where the symbols of “o”, “+”, and “x” represent the results from the simulations with Case (I), (II), and (III), respectively.

Table 1. The value of T_{90} , t_p , and T_{90}/t_p for some identified RS flashes.

GRB	T_{90} (s)	t_p (s)	T_{90}/t_p
GRB 990123 ^a	165.95	44.56	3.72
GRB 041219A ^a	2931.68	1649.68	1.78
GRB 090102 ^a	270.87	60.61	4.47
GRB 090510 ^b	0.24	0.29	0.83
GRB 110731A ^b	1.52	5.49	0.28
GRB 130427A ^a	66.25	14.22	4.66
GRB 130427A ^b	8.99	14.39	0.62
GRB 140512A ^a	706.65	213.39	3.31

^aThe value of T_{90} and t_p are estimated with the optical flash.

^bThe value of T_{90} and t_p are estimated with the *Fermi*-LAT flash.

REFERENCES

- Abbott, B. P., Abbott, R., Abbott, T. D., et al. 2017a, *ApJL*, 848, L12
- Abbott, B. P., Abbott, R., Abbott, T. D., et al. 2017b, *ApJL*, 848, L13
- Abbott, B. P., Abbott, R., Abbott, T. D., et al. 2017c, *Physical Review Letters*, 119, 161101
- Abbott, B. P., Abbott, R., Abbott, T. D., et al. 2017d, *Nature*, 551, 85
- Abbott, B. P., Abbott, R., Abbott, T. D., et al. 2017e, arXiv:1710.09320
- Ackermann, M., Asano, K., Atwood, W. B., et al. 2010, *ApJ*, 716, 1178
- Ackermann, M., Ajello, M., Asano, K., et al. 2013, *ApJ*, 763, 71
- Akerlof, C., Balsano, R., Barthelmy, S., et al. 1999, *Nature*, 398, 400
- Arcavi, I., Hosseinzadeh, G., Howell, D. A., et al. 2017, *Nature*, 551, 64
- Berger, E., Fong, W., & Chornock, R. 2013, *ApJL*, 774, L23
- Blake, C. H., Bloom, J. S., Starr, D. L., et al. 2005, *Nature*, 435, 181
- Coulter, D. A., Kilpatrick, C. D., Siebert, M. R., et al. 2017, *GCN*, 21529
- Deng, W., Li, H., Zhang, B., & Li, S. 2015, *ApJ*, 805, 163
- Dermer, C. D. 2004, *ApJ*, 614, 284
- Dyks, J., Zhang, B., & Fan, Y. Z. 2005, arXiv:astro-ph/0511699
- Fernández, R., & Metzger, B. D. 2016, *Annual Review of Nuclear and Particle Science*, 66, 23
- Fraija, N. 2015, *ApJ*, 804, 105
- Fraija, N., Lee, W., & Veres, P. 2016a, *ApJ*, 818, 190
- Fraija, N., Lee, W. H., Veres, P., & Barniol Duran, R. 2016b, *ApJ*, 831, 22
- Fraija, N., Lee, W. H., Araya, M., et al. 2017, *ApJ*, 848, 94
- Fraija, N., Veres, P., Zhang, B. B., et al. 2017a, arXiv:1705.09311
- Fraija, N., Veres, P., De Colle, F., et al. 2017b, arXiv:1710.08514
- Geng, J.-J., Huang, Y.-F., & Dai, Z.-G. 2017, arXiv:1703.03986
- Goldstein A. e. a., 2017, *GRB Coordinates Network, Circular Service*, No. 21528, #1 (2017), 21528
- Granot, J., Guetta, D., & Gill, R. 2017, *ApJL*, 850, L24
- Hallinan, G., Corsi, A., Mooley, K. P., et al. 2017, arXiv:1710.05435
- He, X.-B., Tam, P.-H. T., & Shen, R.-F. 2017, arXiv:1710.05869
- Hu, L., Wu, X., Andreoni, I., et al. 2017, arXiv:1710.05462
- Huang, Y. F., Gou, L. J., Dai, Z. G., & Lu, T. 2000, *ApJ*, 543, 90
- Huang, X.-L., Xin, L.-P., Yi, S.-X., et al. 2016, *ApJ*, 833, 100
- Kobayashi, S., Zhang, B., Mészáros, P., & Burrows, D. 2007, *ApJ*, 655, 391
- Kumar, P., & Panaitescu, A. 2000, *ApJL*, 541, L51
- Lazzati, D., Perna, R., Morsony, B. J., et al. 2017, arXiv:1712.03237
- Li, L.-X., & Paczyński, B. 1998, *ApJL*, 507, L59
- Lin, D.-B., Mu, H.-J., Lu, R.-J., et al. 2017a, *ApJ*, 840, 95
- Lin, D.-B., Mu, H.-J., Liang, Y.-F., et al. 2017b, *ApJ*, 840, 118
- Lin, D.-B., Huang, B.-Q., Liu, T., et al. 2018, *ApJ*, 852, 136
- Lipunov, V. M., Gorbvskoy, E., Kornilov, V. G., et al. 2017, *ApJL*, 850, L1
- Liu, T., Gu, W.-M., & Zhang, B. 2017, *NewAR*, 79, 1
- Lü, H.-J., Lü, J., Zhong, S.-Q., et al. 2017, *ApJ*, 849, 71
- Lyman, J. D., Lamb, G. P., Levan, A. J., et al. 2018, arXiv:1801.02669
- Ma, S.-B., Lei, W.-H., Gao, H., et al. 2017, arXiv:1710.06318
- Meng, Y.-Z., Geng, J.-J., Zhang, B.-B., et al. 2018, arXiv:1801.01410
- Metzger, B. D., & Berger, E. 2012, *ApJ*, 746, 48
- Murguia-Berthier, A., Ramirez-Ruiz, E., Kilpatrick, C. D., et al. 2017, *ApJL*, 848, L34
- O’Brien, P. T., Willingale, R., Osborne, J., et al. 2006, *ApJ*, 647, 1213
- Rees, M. J., & Mészáros, P. 1994, *ApJL*, 430, L93
- Rhoads, J. E. 1997, *ApJL*, 487, L1
- Rhoads, J. E. 1999, *ApJ*, 525, 737
- Salafia, O. S., Ghisellini, G., Pescalli, A., Ghirlanda, G., & Nappo, F. 2016, *MNRAS*, 461, 3607
- Savchenko, V., Ferrigno, C., Mereghetti, S., et al. 2016, *ApJL*, 820, L36
- Shao, L., & Dai, Z. G. 2005, *ApJ*, 633, 1027
- Shoemaker, I. M., & Murase, K. 2017, arXiv:1710.06427
- Smart, S. J., Chen, T.-W., Jerkstrand, A., et al. 2017, *Nature*, 551, 75
- Soares-Santos, M., Holz, D. E., Annis, J., et al. 2017, *ApJL*, 848, L16
- Song, C.-Y., & Liu, T. 2017, arXiv:1710.00142
- Steele, I. A., Mundell, C. G., Smith, R. J., Kobayashi, S., & Guidorzi, C. 2009, *Nature*, 462, 767
- Tanvir, N. R., Levan, A. J., González-Fernández, C., et al. 2017, *ApJL*, 848, L27
- Troja, E., Piro, L., van Eerten, H., et al. 2017, *Nature*, 551, 71
- Uhm, Z. L., & Zhang, B. 2015, *ApJ*, 808, 33
- Valenti, S., David, Sand, J., et al. 2017, *ApJL*, 848, L24
- Vestrand, W. T., Wozniak, P. R., Wren, J. A., et al. 2005, *Nature*, 435, 178
- Vestrand, W. T., Wren, J. A., Wozniak, P. R., et al. 2006, *Nature*, 442, 172
- Vestrand, W. T., Wren, J. A., Panaitescu, A., et al. 2014, *Science*, 343, 38
- Wang, H., Zhang, F.-W., Wang, Y.-Z., et al. 2017, arXiv:1710.05805
- Wei, J.-J., Zhang, B.-B., Wu, X.-F., et al. 2017, *JCAP*, 11, 035
- Yamazaki, R., Ioka, K., & Nakamura, T. 2003, *ApJ*, 591, 283
- Zhang, B., Fan, Y. Z., Dyks, J., et al. 2006, *ApJ*, 642, 354
- Zhang, B., & Yan, H. 2011, *ApJ*, 726, 90
- Zhang, B.-B., Zhang, B., Castro-Tirado, A. J., et al. 2016, arXiv:1612.03089
- Zhang, B.-B., Zhang, B., Sun, H., et al. 2017, arXiv:1710.05851